


Error Induced by the Optical Path of a High Accuracy and High Bandwidth Optical Current Measurement System

Conference Paper**Author(s):**

Rietmann, Stefan; Biela, Jürgen 

Publication date:

2020

Permanent link:

<https://doi.org/10.3929/ethz-b-000495877>

Rights / license:

[In Copyright - Non-Commercial Use Permitted](#)

Originally published in:

<https://doi.org/10.23919/epe20ecceurope43536.2020.9215673>

Error Induced by the Optical Path of a High Accuracy and High Bandwidth Optical Current Measurement System

Stefan Rietmann and Jürgen Biela
Laboratory for High Power Electronic Systems, ETH Zurich, Switzerland
Physikstrasse 3
8092 Zurich, Switzerland
rietmann@hpe.ee.ethz.ch, jbiela@ethz.ch

Keywords

«Current Sensor», «Measurement», «Device modelling»

Abstract

Birefringence and optical losses in the optical sensor head of a Faraday effect based, high accuracy and high bandwidth current measurement system lead to changes of the polarisation state and orientation. These changes, if not properly determined and calibrated, lead to systematic measurement errors. Therefore, a calibration method for the optical current measurement system focusing on pulse current applications is proposed. The procedure is based on a zero-current measurement and a full (Stokes) polarimeter. It determines the full polarisation state and orientation of a beam propagating through the optical system. The calibration method then allows to determine the parasitic linear birefringence caused by any subsequent optical element in the system. Eventually, an error analysis characterising the potential error reduction by the proposed calibration method is conducted. Further, the additionally introduced error sources caused by the full polarimeter approach are characterised.

1 Introduction

Current measurement systems in high power electronic applications for control and monitoring purposes often require high accuracy and a high measurement bandwidth. A possible solution are magneto-optical current sensors (MOCS) utilizing the Faraday effect for measuring the magnetic field generated by the current. Further advantages of MOCS are their insensitivity to electromagnetic interference and the inherent electrical isolation.

The sensing element, consisting of a magneto-optical (MO) material, is the key element of the current measurement system. Linearly polarised light is incident to this material which turns the plane of polarisation (POP) as function of an applied magnetic field. Choosing the type of material for the sensing element by considering its Verdet constant, optical path length, or optical transmission rate is crucial to achieve the required accuracy and bandwidth as explained in [1].

The integration of the MO material into a sensor head impacts the further behaviour and application spectrum of the current sensor. Intrinsic or all-fiber based sensors have been intensely investigated in the past decades [2, 3, 4, 5]. Due to the long optical path they proved to be rather unsuitable for very high bandwidth applications [1]. Further, the optical fiber needs to be wound around the conductor increasing space demands and impeding practical installation. Extrinsic MOCS systems, as schematically shown in Fig. 1, consist of a dedicated para-, dia- or ferromagnetic bulk material with a short optical path in between the optical fiber guides (up- and downlink).

All MOCS are subject to optically induced errors, in the sensing element, the additional optical fibers and the optical processing elements. These errors arise from linear and circular birefringence, optical losses and environmental influences. Optical error sources in MOCS have been considered in research with special focus on birefringence problems. Solutions to induced and inherent linear birefringence have been addressed especially for all-fiber based MOCS. Potential concepts include the usage of special

fibers and fiber treatment, for instance twisted and annealed single-mode (SM) fibers [2, 4], spun high birefringent fibers (SPUN HiBi) [3], and large fiber loop diameters for low bending induced birefringence [5].

Bulk material based extrinsic setups are less sensitive to bending induced birefringence due to their geometric dimensions. The inherent linear birefringence can be determined with zero field / current calibration measurements and subtracted subsequently. Nevertheless, the additional up- and downlink fibers are sensitive to stress induced birefringence. The downlink, as depicted in Fig. 1, carries the modulated signal and therefore needs special care while designing the sensor head. It is important to either preserve the polarisation information carefully or to gather enough information for a valid reconstruction. Proposed solutions for polarisation preservation are using full integration of the optical processing elements into the sensor head [6, 7, 8, 9] with free-space propagation paths as well as downlink optical fibers for signal propagation [10].

The past research of MOCS and its optical errors focused strongly on all-fiber arrangements and complete preservation of the polarisation state after the modulation. An overall consideration of all polarimetric possibilities for a full polarimetric determination of the SOP and the POP is missing. Hence, the polarisation state measurement and the subsequent translation to a magnetic field or current is usually based on the assumption that only linearly polarised light enters and exits the system with no additional and unintended alteration of the polarisation state or orientation. While this assumption is generally valid for systems assuming a low amount of Faraday rotation ($\leq 10^\circ$), it is rendered invalid by the specification in Tab. I and the concept of multiple full rotations of the POP, used in this project and introduced in [1, 11]. In this paper, optical error sources in a bulk material based extrinsic MOCS are discussed with respect to the accuracy and precision targets as given in Tab. I. With a more precise measurement of the polarisation state, error sources can be identified and isolated during calibration. Hence, an analyser configurations (polarimeter), capable of measuring the complete SOP, is used for the calibration procedure. This calibration process allows then for a significant error reduction.

In section 2, a short summary of optical error sources with focus on birefringence is given. Section 3 proposes a calibration method based on the full characterisation of the SOP and a full polarimetric description of the disruptive part of the optical system. In section 4, an error analysis of the potential error reduction by the calibration method is conducted. Further, the additional error sources introduced by the

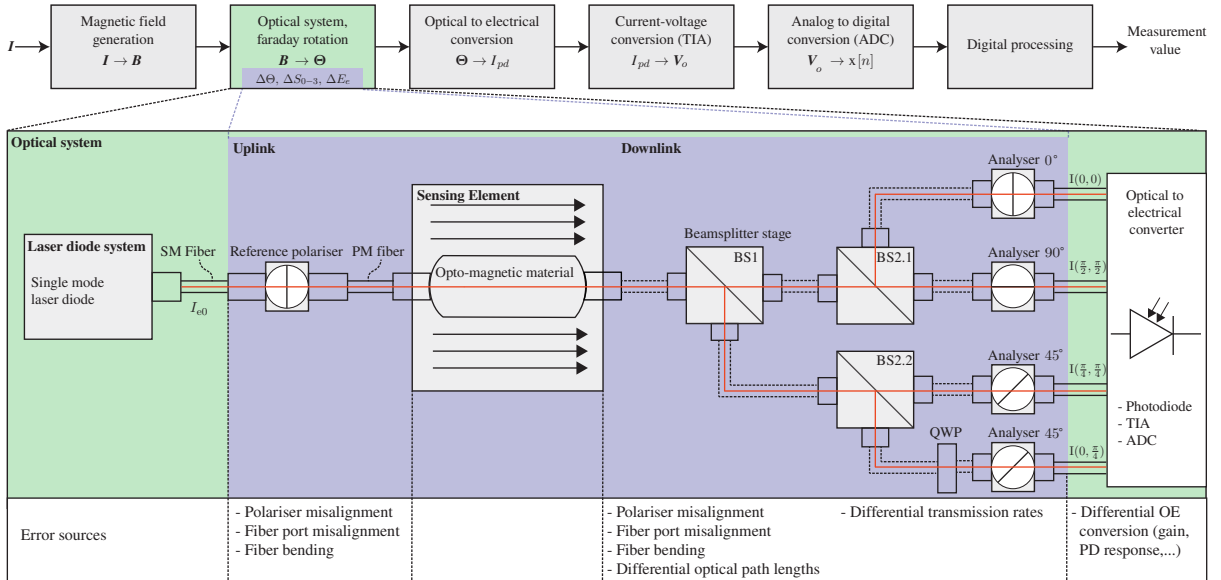


Fig. 1: The optical system of a magneto-optical current sensor is subject to optical losses and birefringence effects. Due to linear and circular birefringence the state of polarisation, the respective optical rotation and the optical intensity of the signal change. Here, the downlink including a full Stokes polarimeter is focused. A calibration procedure reducing the error induced by additional linear birefringence is proposed. Further, an error analysis characterising the possible error reduction but also the additional error introduced by the full polarimeter is conducted.

Table I: Magneto-optical current sensor requirements

Specification	
Current range	100 A ... 10 kA
Frequency bandwidth	DC... ≥ 10 MHz
Measurable pulse rise time (5% - 95%)	< 30 ns...ms
Full bandwidth uncertainty (accuracy)	$< 0.1\%$
Reproducibility error	< 25 ppm

full polarimeter approach are considered. Eventually, the paper concludes in section 5.

2 Optical Error Sources

Induced birefringence in MOCS is one of the most significant sources for systematic errors and measurement imprecisions. It causes changes of the polarisation state and orientation. There, any additional change of the polarisation orientation superposes with the desired change by the applied magnetic field. Depending on the chosen analyser setup, any change of the polarisation state leads to a misinterpretation of the measured output signal, as further elaborated in section 3. Thus, these influences need to be calibrated or prevented in order to increase the accuracy (systematic errors) and precision (random errors). For successfully preventing additional effects in the measurement system, identifying the respective sources is necessary. Since birefringence is present in most of the elements used throughout the optical assembly, it is necessary to specify all elements in terms of their affinity to it.

In the following section, a short definition of birefringence is given. Further, the influence of linear birefringence on the polarisation state and orientation is described with the example of optical fibers.

2.1 Birefringence

2.1.1 Linear Birefringence

Linear birefringence is inherently present in optically anisotropic material, meaning that the material has two different refractive indices (uniaxial case). These materials split an incoming beam into two orthogonally polarised beams, the ordinary and extra-ordinary beam. There, the birefringence of a material is defined as $\Delta n = n_e - n_o$, where n_e and n_o are the refractive indices experienced by the extra-ordinary and the ordinary beam, respectively. Due to the different refractive indices, the phase velocity of the two beams differs, leading to a phase difference described as the linear retardance Δ . As an example, one can assume linearly polarised monochromatic light propagating through birefringent material in z -direction. The polarisation state of the beam is split into the orthogonal polarisation axes as depicted in Fig. 2a. The phase difference between those two orthogonal polarisation components is zero for linearly polarised light. A phase shift is introduced due to the different phase velocities in the x - and y -axes. Hence, the polarisation state is no longer linearly polarised, rather is it elliptically polarised as shown in Fig. 2c

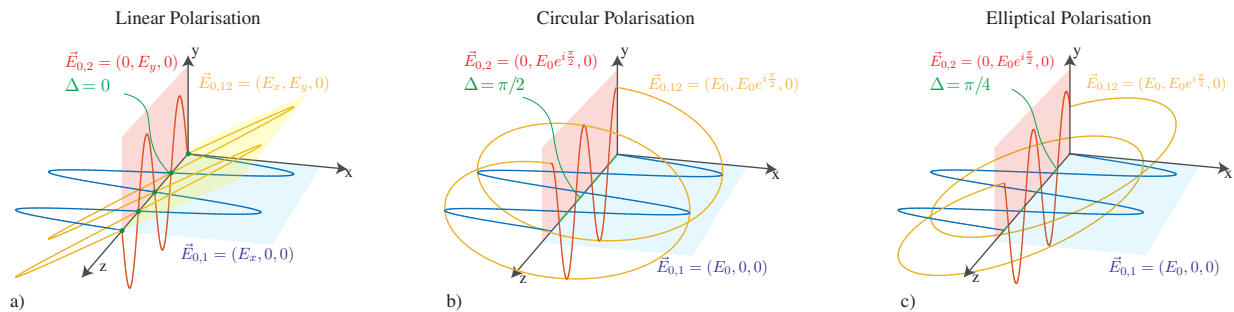


Fig. 2: The polarisation is analytically described with $\vec{E} = \vec{E}_{0,12} \cdot e^{i(kz - \omega t)}$. a) Linear polarisation: The two orthogonal components of the polarisation have a phase difference of $\Delta\varphi = 0$. Depending on the magnitude of the components the orientation of the plane of polarisation is determined. b) Circular polarisation: The two orthogonal components of the polarisation have phase difference of $\Delta\varphi = \pi/2$. c) Elliptical polarisation: The two orthogonal components have phase difference which is not equal to 0 or $\pi/2$.

or, in the special case of a phase shift of $\Delta = \pi/2$, cylindrically polarised as shown in Fig. 2b. As soon as the phase shift reaches a total value of $\Delta = \pi$, the light is linearly polarised again.

2.1.2 Circular Birefringence

Circular birefringence, in opposite to linear birefringence, describes the material induced phase shift between right-hand circular (RHC) and left-hand circular (LHC) polarised waves. Of particular interest for MOCS systems is, that a linearly polarised light beam can be described by the superposition of two counter-rotating circularly polarised waves. The phase difference between those two rotating waves defines the polarisation orientation of the linearly polarised light. For MOCS, inherent circular birefringence can be considered as an offset if present. Hence, calibration of the zero-current field is necessary. Instead of a constant rotation angle, the Faraday rotation in magneto-optical material is essentially considered a magnetic field modulated circular birefringence. It can be described by the circular birefringence [12] with:

$$\Theta = \Theta_{\text{F}}L = \frac{(n^+ - n^-)\pi L}{\lambda} \quad (1)$$

where Θ describes the rotation of the plane of polarisation, n^+ and n^- the refractive index of the RHC and LHC polarisation and L is the length of the optical path. The term Θ_{F} is the Faraday effect specific rotation which is mathematically described with $\Theta_{\text{F}} = \mathcal{V} \cdot |\mathbf{H}|$, where \mathcal{V} is the material specific Verdet constant and \mathbf{H} the magnetic field amplitude in the direction of the optical path [1].

2.2 Optical Components

All of the optical components used in the setup shown in Fig. 1 are subject to inherent or induced, linear or circular birefringence. The magneto-optical material is predominantly subject to the desired magnetic field modulated circular birefringence as described in section 2.1.2. Linear birefringence can be observed in most of the optical elements used in this context, most obviously in optical fibers. There are multiple sources of linear birefringence. Most commonly, linear birefringence is caused by mechanical stress due to bending, temperature fluctuations or vibrations. In the following section, optical fibers serve as an example for the impact of induced linear birefringence.

2.2.1 Optical Fibers

In optical fibers linear birefringence is present both induced and inherent. During manufacturing small defects in the optical fiber and slight core ellipticity lead to inherent linear birefringence [13]. Induced linear birefringence is caused by mechanical stress, for example bending, pressure and force put on the optical fiber. It causes the bending induced retardance Δ_{b} , described in [14] with:

$$\Delta_{\text{b}} = 0.25 \cdot kn^3(p_{11} - p_{12})(1 + \nu)\kappa^2 r^2 \quad (2) \quad \Delta_{\text{b}} = 7.7 \cdot 10^7 \cdot \left(\frac{r}{R}\right)^2 \left[^\circ/\text{m}\right] \quad (3)$$

where n describes the refractive index, p_{ij} are strain optical coefficients, ν the poisson count and r is the optical fiber radius. Further, κ describes the curvature $\kappa = 1/R$ of the bend where R is the curvature radius. For silica based fibers [14] specifies Δ_{b} as in (3). For an optical fiber (e.g. Thorlabs SM600) used at 633 nm with a diameter of 125 μm the minimal long-term bending radius is 25 mm. The bending induced retardance of this particular fiber is around $\Delta_{\text{b}} = 481.3^\circ/\text{m}$ when the fiber is bend to the extent of the maximal allowed radius. A more relaxed bending radius of e.g. 100 mm represents a realistic situation when a fiber is put into a confined space, as for example a box. The bending induced linear retardance for this case is already $\Delta_{\text{b}} \approx 30^\circ/\text{m}$.

The linear retardance, caused by non-ideal optical elements and external influences, changes the overall optical system response. For an accurate measurement a precise description of the influence of linear retardance is necessary.

3 Polarimetric Signal Processing

Converting the polarisation information of the light beam into an electrical signal is an important part of the overall measurement system but also subject to multiple error sources. In particular, the optical error sources, as described in section 2, influence the polarisation state and orientation of the light beam propa-

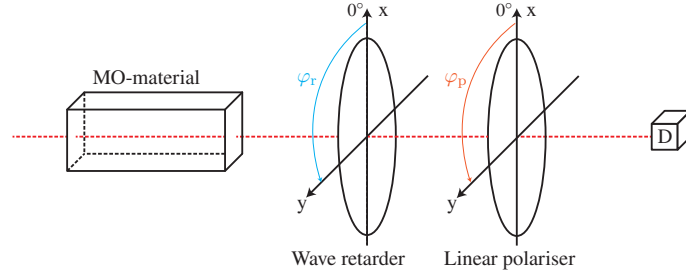


Fig. 3: The schematic figure of the analyser channel shows two rotatable optical elements, a quarter wave plate (QWP) and a linear polariser. The rotation of the relevant axes is indicated by the two parameter φ_r and φ_p , respectively.

gating through the sensor head and the adjacent optical elements. The polarisation state and orientation need to be analysed carefully, in order to identify and isolate the rotation of the plane of polarisation induced only by the current to measure.

In this section, a short introduction to the Stokes and Mueller formalism as well as to basic polarimetric setups is given. These formalism provide the possibility to describe the polarisation state and orientation based on the beam intensity measurements. For detailed information concerning the theory of polarimetric measurement, please be referred to [15, 16, 17] or [18]. Based on these formalisms, an optical system and a calibration procedure to account for the optical errors are proposed.

3.1 Stokes Vector Measurement

For the determination of the polarisation rotation caused by the Faraday effect, a comprehensive mathematical description of the polarisation state and the polarisation orientation is required. The Stokes vector (\vec{S}) in (4) describes the light's polarisation in terms of four parameters. There, S_0 denotes the overall intensity, S_1 the excess of horizontal over vertical polarisation, S_2 the excess of $+45^\circ$ - over -45° -polarisation and S_3 the excess of right-handed circular (RCP) over left-handed circular (LCP) polarisation. Since only the intensity of a beam can be measured directly, the Stokes vector has to be composed by measured intensities altered through analyser settings (Fig. 3) with different angles. The Stokes vector and the associated intensity measurements $I(\varphi_r, \varphi_p)$ are defined by

$$\vec{S} = \begin{pmatrix} S_0 \\ S_1 \\ S_2 \\ S_3 \end{pmatrix} = \begin{pmatrix} E_{0x}^2 + E_{0y}^2 \\ E_{0x}^2 - E_{0y}^2 \\ 2E_{0x}E_{0y}\cos(\delta) \\ 2E_{0x}E_{0y}\cos(\delta) \end{pmatrix} = \begin{pmatrix} I(0,0) + I(\frac{\pi}{2}, \frac{\pi}{2}) \\ I(0,0) - I(\frac{\pi}{2}, \frac{\pi}{2}) \\ 2 \cdot I(\frac{\pi}{4}, \frac{\pi}{4}) - S_0 \\ S_0 - 2 \cdot I(0, \frac{\pi}{4}) \end{pmatrix} \quad (4)$$

where the angle φ_r represents the orientation of a quarter wave plate (QWP) and the angle φ_p represents the orientation of the transmission axis of a linear polariser. A schematic drawing of single analyser channel, which is used for one of the four $I(\varphi_r, \varphi_p)$ measurements, is given in Fig. 3. According to (4), a minimum number of four different intensity measurements are required to fully characterise the polarisation state and orientation of a beam. Measurement concepts with only two analyser channels, as frequently used in MOCS systems (e.g. [19], [11], [20], [21] or [22]), are only able to determine for example the intensities $I(0,0)$ and $I(\frac{\pi}{2}, \frac{\pi}{2})$ from equation (4). Hence, only the deviation from the horizontal polarisation orientation (S_1) and the overall intensity (S_0) can be determined. Thus, the detectable rotation angle range is $0 \leq \theta_{\max} \leq 90^\circ$. However, any polarisation state change towards elliptically polarised states cannot be identified and therefore falsely indicates a change in the polarisation orientation. Hence, a necessary condition for using this measurement setup is the requirement that all light in the system is linearly polarised.

By using an additional analyser channel (e.g. $I(\frac{\pi}{4}, \frac{\pi}{4})$), a full characterisation of the linear plane of polarisation can be achieved. Thus, the detectable rotation angle range enlarges to $0 \leq \theta_{\max} \leq 180^\circ$. There, different measurement arrangements exist, as for example Pickering's or Fessenkov's method [16]. These are primarily used in regular polarimetry (e.g. [16, 18] or [23]) in which the aim is to determine the orientation of a linearly polarised beam with no initial reference and a full mapping of the orientation angle.

By using a fourth analyser channel, the full Stokes vector can be characterised. Since the fourth measurement does not add any information to the polarisation orientation, the detectable rotation angle range remains the same as for the measurement concept using three analyser channels. However, by adding the missing information about the beams ellipticity, it fully characterises the polarisation state. A four-channel or full Stokes polarimeter sets the basis for the following optical system description.

3.2 Optical System Description

While it is important to be able to measure the resulting output beam polarisation \vec{S}_{out} , to identify additional changes in the polarisation, a systematic description of the optical effects in the system is required. This description is eventually necessary in order to distinguish the desired Faraday rotation from these additional polarisation changes in the measured output beam.

In this particular application, the most dominant undesired effect is additional linear birefringence. Its effect can be described in form of a variably rotatable linear retarder, as described in section 2. The change in the index of refraction changes the respective phase velocity of one of the orthogonal waves during propagation through a birefringence afflicted medium. The occurring phase shift affects the polarisation state and orientation by manipulating the Stokes parameter S_1 - S_3 of the outgoing beam. The Mueller matrix $\mathbf{M}_{\text{linRet}}$ characterises the effects on the polarisation of a beam propagating through a linear retarder. The matrix is given in (5):

$$\mathbf{M}_{\text{linRet}} = \begin{bmatrix} 1 & 0 & 0 & 0 \\ 0 & \cos^2 2\varphi + \cos \Delta \sin^2 2\varphi & (1 - \cos \Delta) \sin 2\varphi \cos 2\varphi & -\sin \Delta \sin 2\varphi \\ 0 & (1 - \cos \Delta) \sin 2\varphi \cos 2\varphi & \sin^2 2\varphi + \cos \Delta \cos^2 2\varphi & \sin \Delta \cos 2\varphi \\ 0 & \sin \Delta \sin 2\varphi & -\sin \Delta \cos 2\varphi & \cos \Delta \end{bmatrix} \quad (5)$$

where Δ is the retardance induced by the linear birefringence and φ is the rotation of the reference system on which the retardance is acting. With the Mueller matrix, any combination of n series connected optical elements can be described in terms of an input (\vec{S}_{in}) and output (\vec{S}_{out}) polarisation with the following matrix multiplication:

$$\vec{S}_{\text{out}} = \mathbf{M}_n \cdot \mathbf{M}_{n-1} \cdot \dots \cdot \mathbf{M}_1 \cdot \vec{S}_{\text{in}} \quad (6)$$

Hence, the polarisation related effect in the magneto-optical material and the subsequent optical analyser arrangement can be described with:

$$\vec{S}_{\text{out}} = \mathbf{M}_{\text{linRet}} \cdot \mathbf{M}_{\text{MO}} \cdot \vec{S}_{\text{in}} \quad (7)$$

There, \mathbf{M}_{MO} describes the Faraday effect in the magneto-optical material with:

$$\mathbf{M}_{\text{MO}} = \begin{bmatrix} 1 & 0 & 0 & 0 \\ 0 & \cos 2\theta_F & \sin 2\theta_F & 0 \\ 0 & -\sin 2\theta_F & \cos 2\theta_F & 0 \\ 0 & 0 & 0 & 1 \end{bmatrix} \quad (8)$$

and $\theta_F = \mathcal{V}|B|L$ describes the Faraday effect (\mathcal{V} : Verdet constant, $|B|$: magnetic field flux amplitude, L : optical path length).

Using (7), a description of an optical system influenced by the Faraday effect and by linear birefringence in the magneto-optical material and the subsequent polarimetric analyser is established.

3.3 Linear Birefringence Calibration Procedure

Based on the mathematical model presented in the previous section, a calibration procedure for the MOCS is proposed in the following. Since the considered MOCS is designed for pulse applications, a few basic assumptions can be made:

- The occurrence, time and duration of a pulse event are known.
- The duration of the pulse is finite and relatively short ($\sim \mu\text{s}$) compared to the propagation mecha-

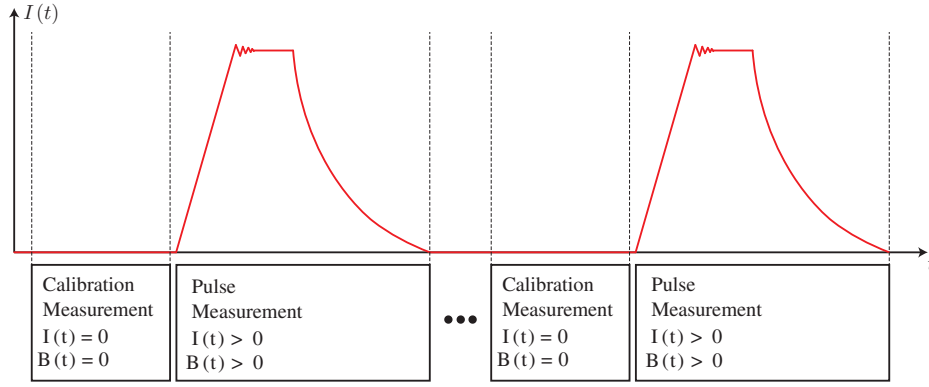


Fig. 4: The calibration measurement allows the detection of the externally applied additional linear birefringence. Assuming pulse current measurements, the environmental influences on the MOCS (movement, temperature, bending) are considered to be constant over the complete measurement time range.

nism of the influences affecting the linear birefringence (movement, temperature, pressure,...).

- The conductor is not conducting any current (i.e. $I_0 = 0$) for a substantial amount of time ($\sim \mu\text{s}$) between two pulses.

With these assumptions it is possible to calibrate the MOCS prior to each pulse and exclude any environmental influences if the input polarisation state is known and the output polarisation state can be fully measured. There, the assumption that linear birefringence generated by environmental effects does not change in the time range between the calibration and the end of the pulse measurement is essential.

With the Mueller matrix in (5) and the system description in (7), the optical system can be approximately described. This system description incorporates the two most dominant effects to the polarisation state and orientation, the Faraday rotation and the additional linear birefringence. During a calibration measurement the conductor must not carry any current (i.e. $I_0 = 0$), essentially resulting in $|B_0| = 0$. Thus, the Mueller matrix for the magneto-optical material is $\mathbf{M}_{MO} = \mathbb{1}$ and the system description reduces to $\vec{S}_{out} = \mathbf{M}_{linRet} \cdot \vec{S}_{in}$. By knowing the output polarisation \vec{S}_{out} from the calibration measurement and with the input polarisation \vec{S}_{in} defined by a reference polariser, the matrix of the additional variably rotatable linear retarder can be determined. With (5), the wanted variables are identified as:

$$\begin{aligned}
 x_1 &= \cos 2\varphi \\
 x_2 &= \sin 2\varphi \\
 x_3 &= \Delta
 \end{aligned} \tag{9}$$

Since the first eigenvector of (5) is already determined, which leads to $S_{out,0} = S_{in,0}$ (no depolarisation assumed), the equation system is reduced to a numerically solvable 3×3 system:

$$\frac{1}{S_{in,0}} \cdot \begin{pmatrix} x_1^2 + x_2^2 \cos(x_3) & [1 - \cos(x_3)]x_1x_2 & x_2 \cdot (-\sin(x_3)) \\ [1 - \cos(x_3)]x_1x_2 & x_2^2 + x_1^2 \cos(x_3) & x_1 \cdot \sin(x_3) \\ x_2 \cdot \sin(x_3) & x_1 \cdot (-\sin(x_3)) & \cos(x_3) \end{pmatrix} \cdot \begin{bmatrix} S_{in,1} \\ S_{in,2} \\ S_{in,3} \end{bmatrix} = \frac{1}{S_{out,0}} \cdot \begin{bmatrix} S_{out,1} \\ S_{out,2} \\ S_{out,3} \end{bmatrix} \tag{10}$$

The retardance Δ is derived directly from the solution for x_3 in (10). The rotation of the reference system φ depends on the two conditions x_1 and x_2 from (9).

By knowing the zero-field / zero-current output polarisation, the deviation caused by the additional linear birefringence in the system can be determined. With this information, this influence can be eliminated in a subsequent pulse measurement and the rotation of the polarisation plane can be identified directly from the output polarisation:

$$\begin{aligned}
 \vec{S}_{out} &= \mathbf{M}_{linRet} \cdot \mathbf{M}_{MO} \cdot \vec{S}_{in} \\
 \Rightarrow \mathbf{M}_{linRet}^{-1} \cdot \vec{S}_{out} &= \mathbf{M}_{MO} \cdot \vec{S}_{in} = \vec{S}_{MO}
 \end{aligned} \tag{11}$$

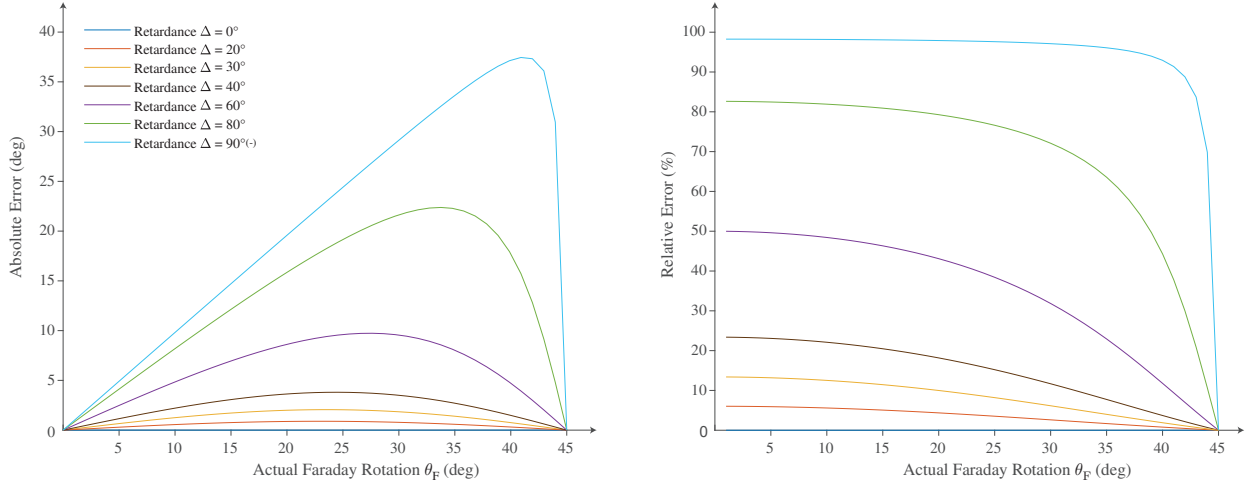


Fig. 5: The potential error range of externally induced additional linear birefringence can lead to a substantial systematic error. The error is periodic over the measurement range of $\theta_F \in [0, \dots, \frac{\pi}{4}]$. Hence, for MOCS with measurement ranges larger than a few degrees a calibration method is necessary.

For the inversion of $\mathbf{M}_{\text{inRet}}$ it needs to be non-singular.

Eventually, the result \vec{S}_{MO} describes the changes caused by the Faraday effect only. From this result, the orientation of the plane of polarisation can be recalculated utilizing the following equation:

$$\theta_F = -\frac{1}{2} \arctan\left(\frac{S_{\text{MO},2}}{S_{\text{MO},1}}\right) \quad \text{with } \text{sgn}(\cos(2\theta_F)) = \text{sgn}(S_{\text{MO},1}) \quad (12)$$

Due to the range of the principal values of the arctan-function the additional condition in (12) is necessary to determine θ_F over the complete range $0 \leq \theta_F \leq \pi$.

4 Error Analysis

In this section, two types of errors are considered for an error analysis. First of all, the error reduction due to the calibration procedure is described and justifies the choice of the full polarimeter approach. The effect of the additional linear birefringence on the beams' polarisation is mathematically removed leaving only the effect of the Faraday rotation. However, the calibration method requires more optical evaluation channels, all of which are subject to production and configuration uncertainties. The numerical example refers to the project requirements stated in Tab. I and a maximal magnetic field amplitude of $|B| = 2\text{ T}$ applied to the MOCS. This results in a total optimal optical rotation of $\theta_{F,\text{max}} = 1980^\circ$. The specification for the magneto-optical material are taken from [1]: $\mathcal{V}_{\text{CdMnTe}} = 150^\circ \text{ T}^{-1} \text{ mm}^{-1}$, $L = 6.6\text{ mm}$.

4.1 Error Reduction by Calibration

The system error ε_θ introduced by the additional linear birefringence is determined with the system description given in (7). It is defined as the difference between the actual Faraday rotation θ_F and the measured (altered) rotation of the polarisation orientation $\theta_{F,\text{alt}}$.

$$\varepsilon_\theta = \theta_F - \theta_{F,\text{alt}} \quad (13)$$

Considering the system description in (7), this error is introduced after the rotation of the polarisation orientation, thus, the measurement result $\theta_{F,\text{alt}}$ depends on the Faraday rotation θ_F itself. Figure 5 shows the dependence of the measurement error on the additional linear birefringence (retardance) and the deflection of the plane of polarisation to the reference axis caused by the Faraday rotation. The minimal and maximal error shows at multiples of $\pi/4$. The error pattern is periodic with $\pi/4$ due to the range and symmetry behaviour of the evaluation equation (11).

In section 2.2.1 the magnitude of bending induced linear birefringence is described with an example

bending radius of 100 mm. For an example single-mode fiber (e.g. Thorlabs SM600) of 1 m operated at 633 nm, the bending induced retardance is $\Delta \approx 30^\circ$. The maximal error for $\theta_F \in [0, \dots, 45]$ is $\varepsilon_\theta = 2.05^\circ$ resulting in a relative error of 9.13% with respect to the single measurement. Considering the above mentioned project requirements and values, the absolute error introduced by this amount of linear birefringence is 2.02 mT or 0.101%, already exceeding the maximal allowed uncertainty. Accordingly, measurements with lower maximal field amplitudes experience higher relative errors. Further, note that the choice of the amount of retardance for this example is arbitrary but reasonable. Higher retardance in the range $\Delta \in [0, \dots, \pi/2]$ will increase the absolute and relative error as well.

By applying the proposed calibration procedure, this error can be eliminated. However, the additional equipment introduces measurement errors, which are taken into account in the following section.

4.2 Polarimeter Error

The uncertainties of commercially available optical elements lead to a deviation of the measured from the expect results. In this analysis, the three channels necessary for the evaluation of θ_F , consisting of three linear polarisers, are considered. The uncertainty of the polariser's orientation influences the intensity measurement in (4), which is necessary for the determination of S_0, S_1 and S_2 . Further, the proposed setup implements three parallel channels. There, the intensity measurement is also influenced by the individual transmission rate of the polarisers.

For the analysis of the error induced by the polariser orientation misalignment, the parameter φ_p in $I(\varphi_r, \varphi_p)$ has to be adjusted by the uncertainty $\Delta\varphi_p$ describing the deflection of the polariser from its optimal orientation. Using the Mueller formalism the polarisers are described with:

$$\mathbf{M}_{\text{Pol}} = \begin{bmatrix} 1 & \cos 2\varphi_p & \sin 2\varphi_p & 0 \\ \cos 2\varphi_p & \cos^2 2\varphi_p & \sin 2\varphi_p \cos 2\varphi_p & 0 \\ \sin 2\varphi_p & \sin 2\varphi_p \cos 2\varphi_p & \sin^2 2\varphi_p & 0 \\ 0 & 0 & 0 & 0 \end{bmatrix} \quad (14)$$

With (6), the Mueller matrix for the polariser (14) and the Mueller matrix for a linear retarder (5) with $\Delta = \frac{\pi}{2}$ (QWP), the optical system describing one analyser channel is given by:

$$\vec{S}_m = \mathbf{M}_{\text{Pol}} \cdot \mathbf{M}_{\text{linRet}} \cdot \vec{S}_{\text{MO}} \quad (15)$$

with \vec{S}_m being the measured output Stokes vector and \vec{S}_{MO} the Stokes vector transmitted from the before described magneto-optical system. From the right-hand term in (4) and the formulation for a general analyser channel (15), the following general formulation for the measured intensity dependent on the polariser's orientation is derived:

$$I(\varphi_r, \varphi_p) = S_{0,\text{MO}} + \cos 2\varphi_r \cdot (S_{1,\text{MO}} \cos^2 2\varphi_p + S_{2,\text{MO}} \cos 2\varphi_p \sin 2\varphi_p - S_{3,\text{MO}} \sin 2\varphi_p) + \quad (16)$$

$$\sin 2\varphi_r \cdot (S_{1,\text{MO}} \cos 2\varphi_p \sin 2\varphi_p + S_{2,\text{MO}} \sin^2 2\varphi_p + S_{3,\text{MO}} \cos 2\varphi_p) \quad (17)$$

Applying the right-hand term of (4) to the formulation for the recalculation of the polarisation orientation in (11) gives a polariser orientation dependent ($\varphi_p, \Delta\varphi_{p,xx}$) formulation (18) for the recalculated polarisation orientation. There, $\Delta\varphi_{p,xx}$ denotes the polariser's individual deviation from the ideal orientation, emphasising that the individual measurement channels are independent from each other.

$$\theta_{F,\text{err}} = -\frac{1}{2} \arctan \left(\frac{2 \cdot I(\frac{\pi}{4}, \frac{\pi}{4} + \Delta\varphi_{p,45}) - I(0, 0 + \Delta\varphi_{p,0}) - I(\frac{\pi}{2}, \frac{\pi}{2} + \Delta\varphi_{p,90})}{I(0, 0 + \Delta\varphi_{p,0}) - I(\frac{\pi}{2}, \frac{\pi}{2} + \Delta\varphi_{p,90})} \right) \quad (18)$$

The maximal measurement error ε_M occurs for a maximal deflection between the polarisers measuring $I(0, 0)$ and $I(\frac{\pi}{2}, \frac{\pi}{2})$. This can be shown by maximising $\varepsilon_M = |\theta_F - \theta_{F,\text{err}}|$.

In this project, as referred to in the beginning of this section, the rotatable polarisers (Thorlabs, FBRP-LPVIS [24]) have a scale allowing for a resolution down to 10 arcmin = 0.167°, hence the reading uncertainty is $\pm 0.083^\circ$. The maximal error calculated with (18) is $\varepsilon_M = 0.101^\circ$. With reference to the

full measurement range of $[0, \dots, 2T]$ the maximal absolute error is 0.1 mT resulting in a relative error of 0.005 %.

For the analysis of the differential transmission losses in the polarisers, the three intensity measurements defining (11) have to be adjusted each by a separate transmission factor. The material thickness dependent transmission rate T is described by the Beer-Lambert law

$$\frac{I}{I_0} = T = e^{-\alpha \cdot d} \quad (19)$$

where α is the absorption coefficient in (m^{-1}) and d is the material thickness in (m). With (19), the transmission factor uncertainty ΔT can be defined as a function of the uncertainty of the material thickness. The maximal absolute error ε_T occurs for the maximal transmission difference between $I(\frac{\pi}{4}, \frac{\pi}{4})$ and the two orthogonal measurements, which can be shown again by maximising $\varepsilon_T = |\theta_F - \theta_{F,\text{err}}|$.

The polarisers used for this project (Thorlabs, FBRP-LPVIS [24]) are made up of a nanoparticle film with a nominal thickness of $d = 250 \mu\text{m}$ and a thickness uncertainty of $\Delta d = \pm 50 \mu\text{m}$. The maximal absolute error is $\varepsilon_T = 1.604^\circ$. With reference to the full measurement range of $[0, \dots, 2T]$ the maximal absolute error is 1.6 mT resulting in a relative error of 0.08 %.

5 Conclusion

In this paper, errors introduced by the optical system in magneto-optical current sensor (MOCS) systems are investigated. Additional linear birefringence superimposed with the modulated measurement signal introduces a large change to the state of polarisation. To resolve the error introduced by the additional linear birefringence a zero-current/zero-field calibration method has been proposed. The calibration method is intended for pulse current measurements and assumes negligible fluctuations of the environmental influences changing the linear birefringence of the optical system. This zero-current calibration measurement is then used to recalculate the actual amount of Faraday rotation based on the complete characterisation of the polarisation state and orientation and the mathematical description of the disruptive optical system.

Depending on the amount of additional linear birefringence, the potential error reduction by using the calibration procedure is substantial. Additional linear retardance of $\Delta = 30^\circ$ already results in an maximal measurement error of 0.101 %. With an increasing amount of linear birefringence the error increases, hence adverse environmental conditions exceed the above given exemplary values substantially.

The additional effort necessary to fully characterise the polarisation state and orientation introduces also new potential error sources. Since multiple optical elements, such as wave retarders and linear polarisers are used in parallel, the differential path losses have to be considered in the final measurement. The differential transmission losses between the analyser channels needs to be considered carefully. Since the given example with off-the-shelf products already amounts to a maximal measurement error of 0.08 %, it is necessary to spend considerable effort designing the analysers channel paths with identical characteristics. This includes the analyser elements (linear polariser, wave retarder) as well as the optical path in terms of fibers, connectors or focal lenses. The measurement error by misalignment of the linear polarisers has also a non negligible impact. However, using highly precise adjustable polarisers allows a significant reduction of this error. The example with the given off-the-shelf products reduces the error already to 0.005 % with respect to the full measurement range.

Acknowledgement

The authors would like to thank CERN for funding the project under contract KE3928/TE. In addition, we would like to thank Dr. M. Barnes and Mr. M.C. Bastos for their valuable scientific input.

References

- [1] S. Rietmann and J. Biela, "Sensor Design for a Current Measurement System with High Bandwidth and High Accuracy Based on the Faraday Effect," in *21st European Conf. on Power Electron. and Appl. (EPE/ECCE Europe)*, 2019.
- [2] S. Rashleigh and R. Ulrich, "Magneto-optic Current Sensing with Birefringent Fibers," *Appl. Phys. Lett.*, vol. 34, no. 11, pp. 768–770, 1979.
- [3] R. I. Laming and D. N. Payne, "Electric Current Sensors Employing Spun Highly Birefringent Optical Fibers," *Journal of Lightw. Technol.*, vol. 7, no. 12, pp. 2084–2094, 1989.
- [4] A. Rose, Z. Ren, and G. W. Day, "Twisting and Annealing Optical Fiber for Current Sensors," *Journal of Lightw. Technol.*, vol. 14, no. 11, pp. 2492–2498, 1996.
- [5] K. Bohnert, P. Gabus, J. Nehring, H. Brandle, and M. G. Brunzel, "Fiber-optic Current Sensor for Electro-winning of Metals," *Journal of Lightw. Technol.*, vol. 25, no. 11, pp. 3602–3609, 2007.
- [6] M. Kanoe, G. Takahashi, T. Sato, M. Higaki, E. Mori, and K. Okumura, "Optical Voltage and Current Measuring System for Electric Power Systems," *IEEE Trans. Power Del.*, vol. 1, no. 1, pp. 91–97, 1986.
- [7] A. Cruden, Z. Richardson, J. McDonald, and I. Andonovic, "Optical Crystal Based Devices for Current and Voltage Measurement," *IEEE Trans. Power Del.*, vol. 10, no. 3, pp. 1217–1223, 1995.
- [8] K. Barczak, "Optical Fibre Current Sensor for Electrical Power Engineering," *Bulletin of the Polish Academy of Sciences: Technical Sciences*, vol. 59, no. 4, pp. 409–414, 2011.
- [9] A. Brigida, I. M. Nascimento, S. Mendonca, J. Costa, M. Martinez, J. M. Baptista, and P. Jorge, "Experimental and Theoretical Analysis of an Optical Current Sensor for High Power Systems," *Photonic Sens.*, vol. 3, no. 1, pp. 26–34, 2013.
- [10] S. Kim, Y.-P. Hong, Y.-G. Kim, and D.-J. Lee, "Field-calibrated Magneto-optic Sensor Based on off-axis Optical probing of Intense Magnetic Fields," *Appl. Opt.*, vol. 56, no. 6, pp. 1701–1707, 2017.
- [11] D. Gerber and J. Biela, "High-dynamic and High-precise Optical Current Measurement System Based on the Faraday Effect," *IEEE Trans. on Plasma Sci.*, vol. 43, no. 10, pp. 3550–3554, 2015.
- [12] J. P. Castera and T. Suzuki, "Magneto-optical Devices," *Digital Encyclopedia of Appl. Phys.*, 2003.
- [13] R. Calvani, R. Caponi, and F. Cisternino, "Polarization Measurements on Single-mode Fibers," *Journal of Lightw. Technol.*, vol. 7, no. 8, pp. 1187–1196, 1989.
- [14] R. Ulrich, S. Rashleigh, and W. Eickhoff, "Bending-induced Birefringence in Single-mode Fibers," *Opt. Lett.*, vol. 5, no. 6, pp. 273–275, 1980.
- [15] E. Collett, *Field Guide to Polarization*. Spie Bellingham, WA, 2005, vol. FG05.
- [16] J. R. Schott, *Fundamentals of Polarimetric Remote Sensing*. Spie Press, 2009, vol. 81.
- [17] H. Fujiwara, *Spectroscopic Ellipsometry: Principles and Applications*. John Wiley & Sons, 2007.
- [18] M. Bass, C. DeCusatis, J. Enoch, V. Lakshminarayanan, G. Li, C. Macdonald, V. Mahajan, and E. Van Stryland, *Handbook of Optics, Volume II: Design, Fabrication and Testing, Sources and Detectors, Radiometry and Photometry*. McGraw-Hill, Inc., 2009.
- [19] B. Chu, Y. Ning, and D. A. Jackson, "Faraday Current Sensor that Uses a Triangular-shaped Bulk-optic Sensing Element," *Opt. letters*, vol. 17, no. 16, pp. 1167–1169, 1992.
- [20] U. Holm, H. Sohlstrom, and T. Brogardh, "YIG-sensor Design for Fibre Optical Magnetic Field Measurements," in *2nd Intl Conf on Optical Fiber Sensors*, vol. 514. International Society for Opt. and Photonics, 1984, Conference Proceedings, pp. 333–336.
- [21] C. Floridia, J. B. Rosolem, and S. Celaschi, "Mitigation of Output Fluctuations due to Residual State of Input Polarization in a Compact Current Sensor," in *Opt. Fiber Sens.* Optical Society of America, 2018.
- [22] P. Mihailovic, S. Petricevic, and R. J., "Improvements in Difference-over-sum Normalization Method for Faraday Effect Magnetic Field Waveforms Measurement," *Journal of Instrumentation*, vol. 1, no. 12, 2006.
- [23] P. Hauge, "Survey of methods for the complete determination of a state of polarization," in *Polarized Light: Instruments, Devices, Applications*, vol. 88. International Society for Optics and Photonics, 1976.
- [24] Thorlabs Inc. (2020, Jun.) FiberBench Polarization Modules, FBRP-LPVIS. [Online]. Available: https://www.thorlabs.com/newgrouppage9.cfm?objectgroup_id=3101